


REVIEW ARTICLE

<https://doi.org/10.1038/s42005-019-0189-6>

OPEN

Towards magnonic devices based on voltage-controlled magnetic anisotropy

Bivas Rana ¹ & YoshiChika Otani ^{1,2}

Despite significant technological advances in miniaturization and operational speed, modern electronic devices suffer from unescapably increasing rates of Joule heating and power consumption. Avoiding these limitations sparked the quest to identify alternative, charge-neutral information carriers. Thus, spin waves, the collective precessional motion of spins in permanent magnets, were proposed as a promising alternative system for encoding information. In order to surpass the speed, efficiency, functionality and integration density of current electronic devices, magnonic devices should be driven by electric-field induced methods. This review highlights recent progress in the development of electric-field-controlled magnonic devices, including present challenges, future perspectives and the scope for further improvement.

Spin waves (SWs) are the dynamic eigen modes of magnetically ordered systems, such as ferromagnetic (FM) metals^{1,2}, ferrimagnetic insulators^{3,4} and antiferromagnets⁵. In other words, SWs are phase coherent collective precessional motion of ordered magnetic spins⁶ (Fig. 1a). These SWs may serve as a potential information carrier in future microwave signal-processing devices, by using its amplitude, phase, and polarization, at significantly lower power consumption as SWs are not associated with translational motion of electronic charges^{4,7}. Therefore, SWs can be used as an alternative to modern charge current-based complementary metal-oxide-semiconductor (CMOS) technology, which is now suffering from increased rate of power consumption due to Joule heating. The quanta of SWs are called “magnon”. Following this name, a new research field, known as “magnonics”^{6,8}, is rapidly developing. When magnonics meets spintronics, the field is known as magnon spintronics⁹. The aim of magnonics is to control and manipulate SW properties so that they can be utilized in future spintronics technology^{8,9}. Apart from lower energy consumption, another advantage of SWs is that they can have wide variety of wavelengths ranging from few tens of micrometer down to few tens of nanometer with the corresponding frequency ranging from few Gigahertz to few Terahertz, which can be even controlled by tuning various internal and external parameters, such as saturation magnetization, various magnetic anisotropies, magnetostatic interactions, exchange interaction, magnetic field, and electric field^{8,10,11}. Although, SWs have much smaller group

¹Center for Emergent Matter Science, RIKEN, 2-1 Hirosawa, Wako 351-0198, Japan. ²Institute for Solid State Physics, University of Tokyo, Kashiwa 277-8581, Japan. Correspondence and requests for materials should be addressed to B.R. (email: bivasranaiid@gmail.com) or to Y.O. (email: yotani@issp.u-tokyo.ac.jp)

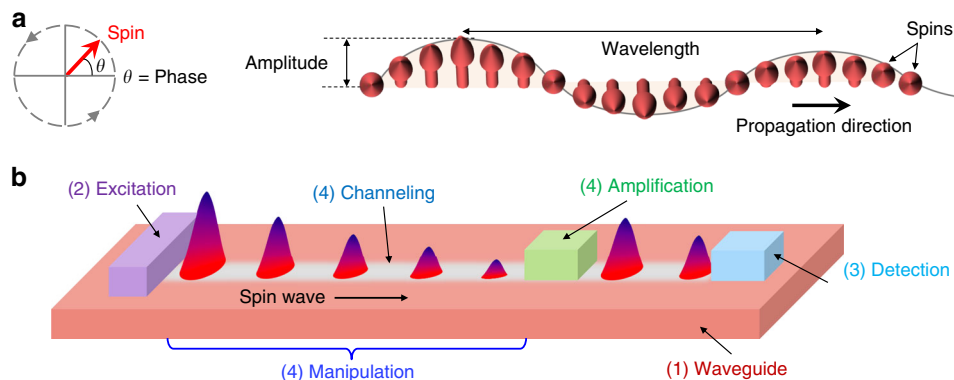


Fig. 1 Spin wave (SW) and magnonic device. **a** Simplified schematic diagram shows rotation of a spin in a circular path and its phase (left panel). SWs are the collective precessional motion of localized magnetic spins coupled with short-range exchange and long-range dipolar interactions (right panel). **b** Schematic illustration shows the basic components of a typical magnonic device. Thin films made of ferromagnetic metals, ferrimagnetic insulators, and antiferromagnets are generally used as SW waveguide, where SWs can be excited by microwave field, spin-orbit torque, pulsed laser beam, and thermal agitation. Those SWs can be detected by various optical or electrical methods. Manipulation and control of SW properties such as frequency, wavevector, phase, group velocity, dispersion character, and guiding SWs through reconfigurable nanochannels are the keys for the development of magnonic devices. SWs can be amplified by compensating damping torque through spin current-induced anti-damping torque

velocity and attenuation length as compared with light waves (i.e. photons) inside optical fiber, shorter wavelength of SWs in nanometer scale makes them compatible with nanoscale magnonic devices as opposed to microscale photonic devices.

Figure 1b shows schematic illustration of a magnonic device. It mainly consists of four elementary components: (1) a spin wave waveguide (SWWG), (2) a microwave source for excitation, (3) a detector, and (4) some functional elements for SW manipulation, channeling, and amplification. Generally, thin films made of ordered magnetic materials are used as SWWGs. Later in this article, we shall describe various methods of SW excitation^{1,12–15}, manipulation^{16–19}, channeling^{17,20–22}, amplification^{2,23–25}, and detection^{14,15,26}. Although different kinds of methods are available for all the above-mentioned operations, all-electrical methods are preferable for application of magnonics into on-chip-integrated devices. However, charge current-based electrical methods, which are most commonly found in the literatures for operating magnonic devices, cannot be used because of high power consumption due to Joule heating, which becomes more severe for nanoscale devices. For successful implementation of magnonic devices into future technology, we need to find out energetically efficient alternative method for their operation, which must be compatible with nanoscale microwave devices. This can be achieved if magnonic devices are operated by voltage i.e., electric field instead of charge current. Magnetoelectric (ME) effect allows us to control magnetic properties by electric field. Multiferroic materials show strong ME effect due to presence of magnetic and electrical ordering, simultaneously^{27,28}. The strong coupling between magnetic and electric polarization allows to control magnetic properties by electric field and vice versa. However, multiferroic materials generally have low saturation magnetization, low spin polarization and there are only few single-phase multiferroic materials available at room temperature as opposed to FM materials²⁹. Although, ferromagnetic semiconductors³⁰, such as (In, Mn)As, (Ga, Mn)As, also offer electric field modulation of magnetic anisotropy and exchange interaction via electric-field-controlled carrier density, room temperature operation has not been demonstrated yet. Alternatively, ME effect can be observed when a magnetostrictive film (e.g. Ni) is placed on a piezoelectric substrate (e.g. $\text{Pb}(\text{Mg}_{1/3}\text{Nb}_{2/3})\text{O}_3$ – PbTiO_3 , LiNbO_3)³¹. The electric field-induced strain in the piezoelectric substrate is transferred to adjacent FM film, in which the magnetic properties are modulated through magnetostriction. For

practical applications, piezoelectric thin films are required instead of the piezoelectric substrate. However, there is no report on piezoelectric films with strong ME effect until now. Another alternative method would be recently discovered voltage (i.e., electric field) controlled magnetic anisotropy (VCMA), which is generally observed at the interface between ultrathin $3d$ transition ferromagnetic metals (e.g., Fe, CoFeB) and nonmagnetic insulators (e.g. MgO , Al_2O_3)³². This VCMA is believed to be occurred due to relative changes of electronic occupation state in $3d$ orbitals of FM^{33,34} by applied electric field.

In this article, we review the recent progress of electric-field-controlled magnonic devices based on propagating SWs in ferromagnetic thin films. After a brief historical background about various methods for excitation, manipulation, channeling, amplification of SWs, and development of magnonic crystals and logic gates, we highlight recent reports on the operation of various functions of magnonic devices by voltage i.e., electric field, in particular, through modulation of perpendicular magnetic anisotropy at ferromagnetic metal and oxide interface. Finally, we describe the future perspectives, challenges, and further scopes to improve the efficiency of magnonic devices.

Origin of VCMA and VCMA coefficient

Perpendicular magnetic anisotropy (PMA) is essential to enhance the thermal stability of nanomagnets at room temperature. Generally, strong PMA is observed at the interfaces between $3d$ transition metal FMs (e.g., Co) and heavy nonmagnetic metals (e.g., Pt, Pd, W, Au)³⁵. However, Co–Pt, Co–Pd, and Co–Au heterostructures also show relatively high Gilbert damping, which is not desirable for current-induced magnetization switching and other magnonics applications. Moreover, interfacial PMA (iPMA) cannot be modulated by electric field in these systems due to the absence of oxide or dielectric layer at the interface. PMA can also be observed at the interfaces between $3d$ -FMs (e.g. Co, Fe, and their alloys) and MO_x ($M = \text{Mg}$, Al, Ta, and Ru). Among them, the heterostructures made from CoFeB and MgO draw particular attention due to lower damping constant of CoFeB³⁶ and high tunneling magnetoresistance (TMR) ratio of CoFeB/MgO/CoFeB at room temperature³⁷. At CoFeB/MgO interface, the out-of-plane (OOP) $3d_z^2$ -orbitals of Fe strongly bond with OOP $2p_z$ -orbitals of O resulting in a significant charge transfer from $3d_z^2$ -orbitals to $2p_z$ -orbitals. Therefore, the number of electrons in

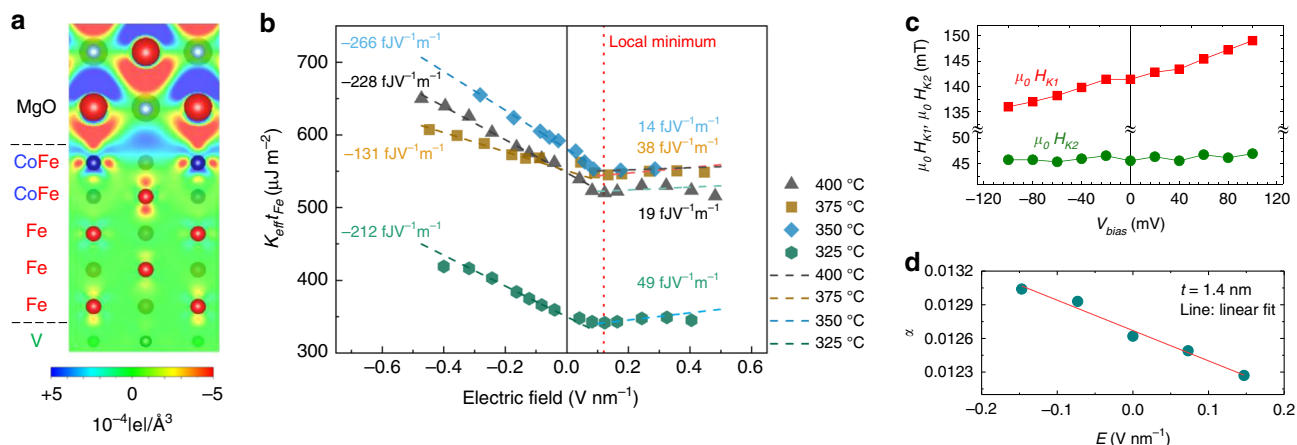


Fig. 2 Origin of voltage-controlled magnetic anisotropy (VCMA) and VCMA coefficient. **a** First-principle calculation result shows the induced charge density at ferromagnet (FM)/oxide interface at bias electric field $E = +0.2 \text{ V nm}^{-1}$ with respect to $E = -0.2 \text{ V nm}^{-1}$. The blue and red color scale represents the accumulation and depletion of holes, respectively³⁸. Reproduced with the permission from <https://doi.org/10.1103/PhysRevB.96.220412>. **b** Areal density of interfacial perpendicular magnetic anisotropy (iPMA) as a function of E for different annealing temperatures. Nonlinear behavior of VCMA and local minima of iPMA are observed⁴² at $E = +100 \text{ mV nm}^{-1}$. Reproduced with permission from Xiang, Q., Wen, Z., Sukegawa, H., Kasai, S., Seki, T., Kubota, T., Takanashi, K., Mitani, S. Nonlinear electric field effect on perpendicular magnetic anisotropy (PMA) in Fe/MgO interfaces, *J. Phys. D: Appl. Phys.* **50**, 40, 40LT04 (2017). <https://doi.org/10.1088/1361-6463/aa87ab> © IOP Publishing. Reproduced with permission. All rights reserved. **c** Variation of first- and second-order perpendicular magnetic anisotropy fields are shown as a function of bias voltage⁴³. Reprinted from Kanai, S., Gajek, M., Worledge, D. C., Matsukura, F. & Ohno, H. Electric field-induced ferromagnetic resonance in a CoFeB/MgO magnetic tunnel junction under dc bias voltages. *Appl. Phys. Lett.* **105**, 242409 (2014), with the permission of AIP Publishing. **d** Variation of Gilbert damping constant with E ⁴⁴. Reprinted from Okada, A., Kanai, S., Yamanouchi, M., Ikeda, S., Matsukura, F., Ohno, H. Electric-field effects on magnetic anisotropy and damping constant in Ta/CoFeB/MgO investigated by ferromagnetic resonance, *Appl. Phys. Lett.* **105**, 052415 (2014), with the permission of AIP Publishing

OOP orbitals is reduced as compared with the number of electrons in in-plane (IP) orbitals, which in fact introduces a sizeable PMA through spin-orbit coupling (SOC) of FM. When electric field is applied at FM/oxide interface, the number of electrons in OOP $3d$ -orbitals of Fe is changed with respect to IP orbitals as shown from first-principle calculations^{33,38} (Fig. 2a). This affects the bonding strength between $3d$ - and $2p$ -orbitals resulting in a substantial change of iPMA. Since the penetration depth of electric field in metal is only few Å, therefore VCMA effect is only limited to ultrathin FM films. Although, electric field control of electronic occupation state is believed to be the main mechanism behind VCMA, several alternative theories are also found in the literature. One of the interesting theories says that the inhomogeneous electric field at the metal/oxide interface couples to the quadrupole of electronic orbital in FM³⁹. This electric quadrupole again couples to the magnetic dipoles and controls iPMA. Another theory says that Rashba SOC at FM/oxide interface can generate iPMA⁴⁰. The applied electric field at the interface modifies Rashba SOC, which in fact modulates iPMA. Naik et al. experimentally demonstrated the development of tensile and compressive strain in nanometer thick MgO layer due to the application of electric field with opposite polarity at FM/oxide interface⁴¹. Therefore, it is possible that the iPMA is modulated by the piezoelectric property of MgO through magneto-elastic coupling. In reality, all the above mechanisms may be present and contribute simultaneously to the modulation of iPMA. Moreover, these mechanisms neither require atomic movement nor require any chemical reaction, which enables high-speed operation of VCMA magnonics devices with high-cycling endurance.

First-principle calculation shows that the change in the number of electrons in $3d$ -orbitals of Fe is linearly proportional to the applied electric field (E) at FM/oxide interface³⁴. Therefore, change in the magnetic moment and iPMA should also be linearly proportional to electric field³³ i.e., $\Delta K_S = \beta E$, where ΔK_S is the change in iPMA and β is known as magnetolectric or VCMA

coefficient. Several experimental reports show this linear variation of iPMA with electric field^{45–47}. However, the magnitude and sign of β depend upon several factors. For instance, VCMA coefficient and its sign can be same or different for opposite polarity of electric field^{46–49}. Xiang et al. reported nonlinear variation of iPMA with electric field for Cr/Fe/MgO heterostructure⁴² with a local minima of iPMA at $E = +100 \text{ mV nm}^{-1}$ (Fig. 2b). The iPMA increases linearly with E above and below the local minima. Although minimal point is independent of annealing and measurement temperature, β and iPMA strongly depend upon them. These behaviors can be attributed to have intrinsic origin due to electronic band structure at the FM/oxide interface. Some additional reports show that β also depends upon the underlayer material^{45,50}, substrate⁵¹, temperature⁵², FM layer⁴⁴, and MgO overlayer thickness⁵³. This is worth to mention here that only first-order anisotropy varies with electric field, whereas second-order anisotropy remains unchanged^{43,44} (Fig. 2c). That means only first-order anisotropy has interfacial origin. Interestingly, the electric field applied at the FM/oxide interface not only changes the iPMA but also modulates Gilbert damping parameter (Fig. 2d) as demonstrated by Okada et al.⁴⁴. This is because iPMA and Gilbert damping, both, are originated from SOC. Surprisingly, any correlation between VCMA coefficient and electric field variation of Gilbert damping was not observed.

The reported value of β is up to few tens of $\text{fJ V}^{-1} \text{m}^{-1}$ for CoFeB/MgO interface^{44,47,50}. One of the challenges is to increase the value of β in order to further improve the efficiency of magnonics devices. This can be done by engineering FM/oxide interface. Theoretical reports⁵⁴ predict that the insertion of the ultrathin heavy metallic layer in between FM and oxide layer could significantly enhance the value of β . Later on a number of experimental reports came out to show the enhancement β by inserting even relatively lighter materials, such as Hf, Mg⁵⁵, and heavy materials, such as Ta, Pt⁵⁵, W, and Ir⁵⁶. The possible reason behind this is the suppression of surface oxidation of FM

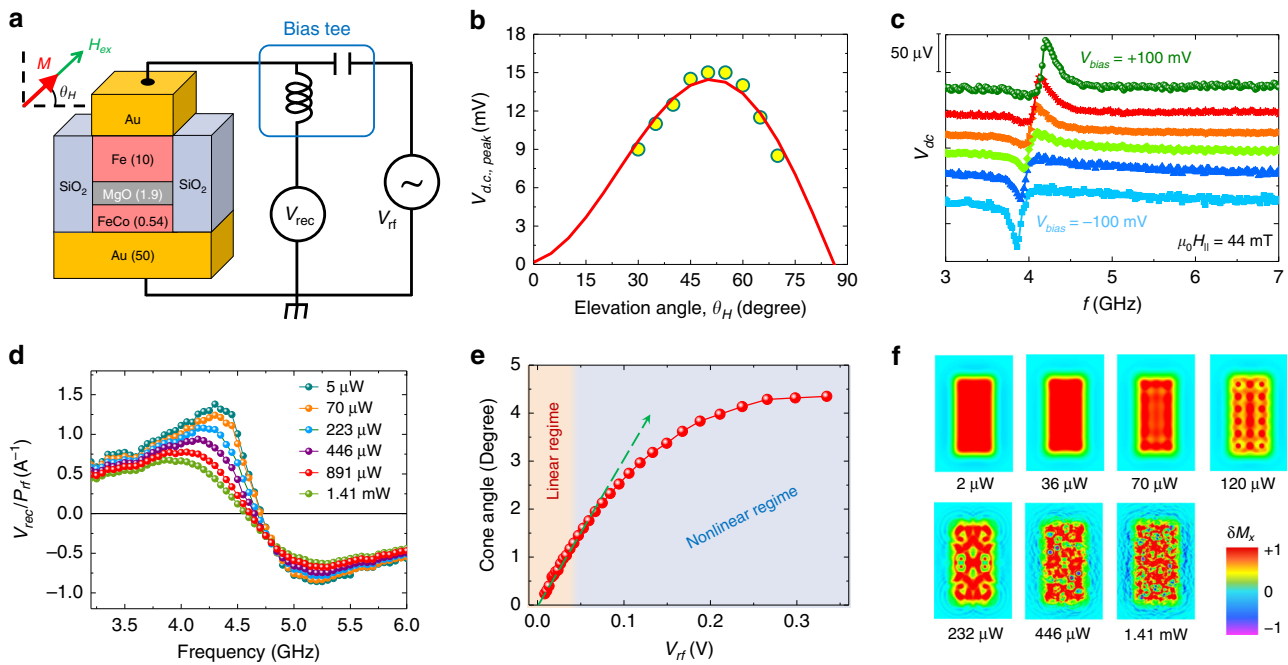


Fig. 3 Excitation of ferromagnetic resonance (FMR) by voltage-controlled magnetic anisotropy (VCMA). **a** Schematic diagram of a magnetic tunnel junction (MTJ) and measurement set up for homodyne detection of VCMA-FMR⁶³. **b** Elevation angle dependence of VCMA-FMR signal measured by MTJ⁶³. Adapted by permission from Nature Publishing Group: Nature Physics, Electric-field-induced ferromagnetic resonance excitation in an ultrathin ferromagnetic metal layer, Nozaki, T., Shiota, Y., Miwa, S., Murakami, S., Bonell, F., Ishibashi, S., Kubota, H., Yakushiji, K., Saruya, T., Fukushima, A., Yuasa, S., Shinjo, T., Suzuki, Y., copyright 2012. **c** Change of VCMA-FMR lineshape with bias voltage⁴³. Reprinted from Kanai, S., Gajek, M., Worledge, D. C., Matsukura, F. & Ohno, H. Electric field-induced ferromagnetic resonance in a CoFeB/MgO magnetic tunnel junction under dc bias voltages. *Appl. Phys. Lett.* **105**, 242409 (2014), with the permission of AIP Publishing. **d** Rectified voltage (V_{rec}), rescaled by microwave power (P_{rf}), is plotted as a function of frequency for different values of P_{rf} . **e** Variation of cone angle of magnetization precession with V_{rf} . **f** Simulated spatial maps of dynamic magnetization show the transition from coherent FMR to incoherent FMR above threshold microwave power⁴⁷ (licensed under CC BY 4.0)

layer and modification of FM-3d & O-2p hybridization. Few reports also show that the doping of heavy metals like Ir⁵⁷ and Cr⁴⁹ at the FM/oxide interface can significantly enhance, both, iPMA and β . The VCMA coefficient over few hundreds of $\text{fJ V}^{-1}\text{m}^{-1}$ can be achieved by this method due to the diffusion of Ir, Cr into the FM layer. VCMA coefficient can be further increased up to few $\text{pJ V}^{-1}\text{m}^{-1}$ by using voltage-controlled electromigration⁵⁸, redox reactions⁵⁹, charge trapping⁶⁰, and magnetostriction⁶¹. Unfortunately, these methods of VCMA are not suitable for high-frequency applications due to lower speed of operation and poor cycling endurance. Therefore, engineering the electronic bands at FM/oxide interface is more desirable for microwave magnonic devices.

VCMA-induced ferromagnetic resonance (VCMA-FMR)

As VCMA at FM/oxide interfaces relies upon the modification of electronic occupation states in 3d orbitals of FM, it is suitable for microwave applications, such as excitation of ferromagnetic resonance (FMR) and SWs in the gigahertz regime. There are several important characteristics of VCMA excitation of FMR (VCMA-FMR). One of the most promising and sensitive methods for electrical detection of VCMA-FMR is the homodyne detection technique by using TMR effect^{47,62,63} (Fig. 3a). A magnetic tunnel junction (MTJ) composed of a free magnetic layer and a reference or pinned magnetic layer is used for this purpose. Microwave voltage is applied across the MTJ to periodically modulate the iPMA of free layer. At resonance, a finite dc voltage V_{rec} (called rectified voltage) is produced across the MTJ due to mixing of time varying TMR and small radio frequency (rf) current across the junction. One of the basic differences between spin-transfer torque (STT) excitation and VCMA excitation is that the STT is

proportional to $\sin \theta$, whereas VCMA-torque is proportional to $\sin \theta \cos \theta$, where θ is the elevation angle of magnetization⁶³. Therefore, V_{rec} becomes proportional to $\sin^2 \theta$ for STT excitation and $\sin^2 \theta \cos \theta$ for VCMA excitation when measured by MTJ, as the sensitivity of TMR detection is proportional to $\sin \theta$. Hence, VCMA-FMR signal measured by MTJ becomes maximum at $\theta = 55^\circ$ (Fig. 3b). It is important to mention here that the pinned layer does not have any role for VCMA excitation, it is used only for detection. In absence of STT and/or field-like torque (FLT), the lineshape of the VCMA-FMR spectra should be purely anti-symmetric Lorentzian. However, as the homodyne detection signal is sensitive to the relative phase between rf current through the MTJ and time varying TMR due to FMR, the lineshape can be changed from anti-symmetric Lorentzian to symmetric Lorentzian depending upon the relative orientation of magnetizations in two layers of MTJ⁶⁴ and DC bias voltage⁴³ (Fig. 3c). Moreover, the sign of the anti-symmetric Lorentzian signal can be reversed by reversing the direction of bias magnetic field⁶².

Most important advantage of VCMA-FMR is ultralow power consumption. Nozaki et al.⁶³ have shown that the power consumption for VCMA excitation can be at least two orders of magnitude lower than the current induced STT excitation. It is worth to mention here that this is not the fundamental limit of power consumption for VCMA-FMR. The power consumption can be further reduced by increasing VCMA coefficient through engineering of FM/oxide interface. At lower excitation power or in the linear regime of excitation, V_{rec} is proportional to applied rf power (P_{rf})⁶³, whereas cone angle of magnetization precession is linearly proportional to applied rf voltage (V_{rf})⁴⁷. Moreover, the lineshape, linewidth, and resonance frequency of VCMA-FMR remain independent of P_{rf} . However, with the increase of P_{rf} , the

V_{rec} , and cone angle of precession deviate from their linear increment with P_{rf} and V_{rf} , respectively, due to the nonlinear FMR^{47,65} (Fig. 3d, e). Therefore, the lineshape is distorted from anti-symmetric Lorentzian, linewidth is broadened, and resonance frequency is decreased (Fig. 3d). Rana et al.⁴⁷ have shown that the coherent FMR becomes incoherent above a threshold excitation power (Fig. 3f), which in fact distorts the lineshape and increases the linewidth. Cone angle of magnetization precession monotonically increases with P_{rf} and eventually becomes saturated. In the nonlinear regime, FMR is basically governed by four magnon scattering, which creates two $k \neq 0$ ($+k$ and $-k$) magnons by annihilating two $k = 0$ magnons⁶⁶. As a result, coherent FMR becomes incoherent.

Nonlinear parametric excitation of SWs by VCMA

Uniform FMR and also coherent SWs cannot be excited by VCMA when the static magnetization of FM film is aligned either perpendicular to the film plane ($\theta = 90^\circ$) or in the film plane ($\theta = 0^\circ$) (Fig. 3b). However, by performing theoretical analysis^{67,68} and numerical simulations⁶⁹, Verba et al. have shown that these special magnetization configurations are suitable for nonlinear parametric excitation of SWs, where frequency of applied rf electric field (E_{rf}) i.e., VCMA is twice larger than the SW frequency. Later on it has been experimentally demonstrated by Chen et al.⁷⁰. The magnetization vectors of a FM film generally precess randomly around its equilibrium direction due to the thermal fluctuation (thermally generated magnons). When the oscillation trajectory becomes elliptical due to presence of either shape anisotropy or magnetocrystalline anisotropy of the FM film, the z -component of dynamic magnetization oscillates in a frequency twice larger than the magnetization vector oscillation⁶⁷. The time varying VCMA efficiently couples to the z -component of dynamic magnetization when the frequency of applied E_{rf} becomes twice larger than the SW frequency. The main advantage of parametric excitation is that it can efficiently excite and selectively amplify even shorter wavelength SWs as compared with linear excitation, where the wavelength of excitation is limited by the dimension of gate electrode and excitation efficiency drastically decreases for shorter wavelengths¹. Of course this limitation of linear excitation may be overcome by the methods mentioned in ref. ⁷¹. Interestingly, parametric SWs with relatively large amplitude and much narrower linewidth can be excited by VCMA⁶⁹, as compared with Oersted field. The disadvantage of parametric excitation, as opposed to linear excitation, is that it is not energy efficient as high-threshold power of microwave field is required for the excitation. The threshold power strongly depends upon the width of waveguide (WG), width of gate electrode, excitation frequency, and SW wavevector^{67,68}. Nevertheless, the threshold power can be significantly reduced by replacing microwave field by VCMA⁷⁰. For OOP orientation of magnetization, the lower threshold value of excitation is obtained for long wavelength dipolar dominated SWs in narrow WG with width about few tens of nanometer⁶⁷ (Fig. 4a). For IP orientation of magnetization, the SW with much shorter wavelength (dominated by exchange interaction) can be excited very efficiently by VCMA (Fig. 4b), as the efficiency of parametric interaction between excited SWs and VCMA is proportional to OOP component of dynamic magnetization in this case⁶⁸. Herein lies the advantage of VCMA excitation over Oersted field excitation, as this is only the inherent property of VCMA excitation. In all the cases, the threshold power can even be reduced by choosing a FM/oxide heterostructures with higher VCMA coefficient. Another important characteristic of parametric excitation is that the resonance frequency shifts toward the lower frequency with the increase of excitation power due to nonlinear effect⁷⁰ (Fig. 4c).

Excitation of coherent propagating SWs

There are several ways available for the excitation of SWs, such as rf current-induced Oersted fields^{14,19} (Fig. 5a), spin-transfer torques (STT)^{12,13} (Fig. 5b), femtosecond pulsed laser beams^{11,15,72-74} (Fig. 5c), and thermal energy⁷⁵. Oersted fields are not suitable for nanoscale spintronics devices due to their spatially nonlocalized nature. However, there are some alternative ways which even enable spatially uniform microwave Oersted fields to excite SWs with shorter wavelength without localizing it. For instance, SWs with shorter wavelength can be excited by creating magnetic nonuniformities either naturally or artificially. Au et al. have shown that localized dynamic dipolar field created by the FMR of a rod-like magnetic nanostructure on top of a SWWG can excite shorter wavelength SWs⁷⁶. Even smooth interface between two magnetic films can also excite short-wavelength coherent SWs very efficiently⁷¹. All these above-mentioned methods either need to create nonuniformities in magnetic film or need two magnetic layers, which may increase the complexity of device fabrication. The STT, on the other hand, can be easily localized in nanoscale area. However, these current-induced methods suffer from huge power consumption due to inherent Joule heating. Another efficient way to excite coherent SWs is femtosecond pulsed laser beam^{11,15}. But this method is suitable only for scientific studies, and may be difficult to implement in practical magnonic devices. Thermal excitations are also not suitable for practical purposes due to its incoherent nature of excitation. As an alternative VCMA promises to be a very efficient way to excite FMR and SWs at ultralow power consumptions. The key advantage of VCMA is that the excitation area can be localized without creating nonuniformities in magnetic structure or using a second magnetic layer, unlike Oersted field excitation.

Although parametrically excited nonlinear SWs have several advantages, linear or coherent propagating SWs are required for the development of magnonic logic devices. This is because the linear relationship of SW amplitude with rf voltage (V_{rf}) of excitation makes it easier to control SW amplitude and phase for logic operation. Rana et al.¹ have experimentally demonstrated that coherent propagating SWs can be excited in ultrathin FM films by VCMA. In this case, a metal gate electrode is placed on the top of the oxide layer (Fig. 5d). V_{rf} is applied across gate electrode and WG for periodically modulating iPMA of WG underneath gate electrode. At resonance frequency, the coherent SWs with frequency same as V_{rf} are excited and propagate along the WG. The lateral width (w) of the gate electrode decides the range of wavevectors, which can be excited by V_{rf} . The excitation efficiency as a function of wavevector can be found by performing the Fourier transform of spatial distribution of electric field at the FM/oxide interface. In this case, the dependence of excitation efficiency with wavevector is given by square of sinc function, which says that the SWs with wavevector (k) up to $2\pi/w$ can be excited¹. Therefore, in order to excite SWs with high k (i.e., shorter wavelength), the width w of gate electrode needs to be reduced. Nevertheless, this is technically possible as nanometer-scale gate electrode can be fabricated and electric field can be, in principle, localized within few tens of nanometer underneath gate electrode.

The SW propagation length in metallic FM films is limited to few micrometer to few tens of micrometer due to higher Gilbert damping as opposed to ferrimagnetic insulators (e.g., Yttrium iron garnet (YIG)) and Heusler alloys. The SW propagation length for ultrathin FM films possessing iPMA is further reduced to about a micrometer due to lower group velocity and higher Gilbert damping parameter. Therefore, one of the challenges of magnonics is to increase the propagation length of SWs in ultrathin FM films. Although, several charge current-induced SW

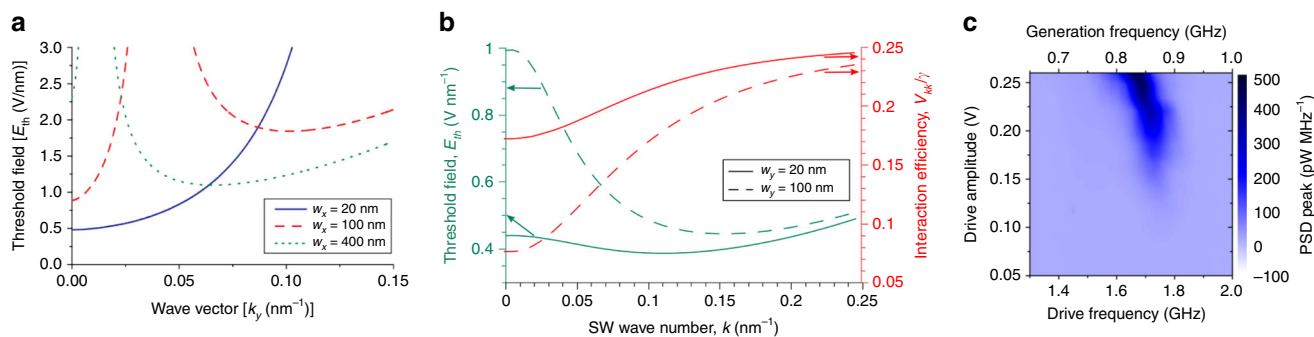


Fig. 4 Nonlinear parametric excitation. Threshold value of radio frequency electric field (E_{rf}) as a function of spin wave (SW) wavevector k for different widths of waveguide (WG) with magnetization vector aligned along, **a** out-of-plane direction⁶⁷, reproduced with the permission from <https://doi.org/10.1103/PhysRevApplied.1.044006>, and, **b** in-plane direction⁶⁸ of thin film, reproduced with the permission from <https://doi.org/10.1103/PhysRevApplied.7.064023>. **c** Experimentally measured power spectral density (PSD) as a function of frequency and amplitude of E_{rf} (ref. ⁷⁰). Reprinted with the permission from Chen, Y., Lee, H. K., Verba, R., Katine, J. A., Barsukov, I., Tiberkevich, V., Xiao, J. Q., Slavin, A. N., Krivorotov, I. N., Parametric resonance of magnetization excited by electric field. *Nano Lett.* **17**, 572–577 (2017). Copyright 2017 American Chemical Society

amplification methods^{2,3,23,24,77} are available, the main drawback of these methods is, again, Joule heating and higher power consumption. Alternatively, this problem can be solved by reducing the overall dimension of the device below SW propagation length. One necessary condition for this is that the excitation area should be strictly localized within nanometer dimension in order to fit with nanoscale devices. Herein lies the advantage of VCMA excitation of SWs over microwave antenna-induced Oersted field excitation. Rana et al. have shown that amplitude of VCMA-induced SWs decay exponentially as a function of propagation distance due to localized nature of electric field underneath the gate electrode¹. On the other hand, antenna-induced SWs do not exactly follow exponential decay function, specially, first couple of points, due to nonlocalized nature of antenna-induced Oersted field (Fig. 5e). This proves that VCMA-induced excitation (linear and nonlinear) will be more suitable for nanoscale magnonic devices, especially, for ultrathin FM films. The amplitude of VCMA-induced coherent SWs also vary linearly with V_{rf} (Fig. 5f)¹. Also, there is not any threshold power of linear coherent excitation unlike nonlinear parametric excitation. That means coherent SWs can be excited even at ultralow microwave power like uniform FMR, with a scope of further reduction by increasing VCMA coefficient.

Formation of reconfigurable SW nanochannels

After excitation, the SWs propagate along the surface of WG. For practical application, it is necessary to guide the SWs through channels so that they can reach to a targeted position for next operation. One of the popular methods is geometrically patterning the WG either into stripe or wire⁷⁸. In this case, the SW path is basically decided by the shape of the WG, which cannot be further manipulated. Second method is the confinement of SWs by internal demagnetizing field of WG⁷⁹ (Fig. 6a). The SW path can be moved from the edge to the center of WG and vice versa simply by tuning the excitation frequency. When the magnetostatic SWs propagate from a narrow WG to a wider WG, it does not propagate along a straight line. Instead, SWs are bended and propagate like a beam along well-defined directions due to the anisotropic nature of dipolar interaction (Fig. 6b). This is called SW caustic. The direction of SW propagation can be controlled by changing the orientation of in-plane bias magnetic field²⁰. The situation becomes even more interesting in the presence of nonuniform magnetization i.e., nonuniform effective magnetic field inside the WG, which behaves like a graded refractive index for the propagation of magnetostatic SWs. The SWs, passing

through the nonuniformly magnetized area, can be steered toward preferred direction by tuning nonuniformity of internal magnetic field with an external magnetic field⁸⁰. In principle, any patterned magnetic micro-or-nanostructure shows non-uniformity in magnetization. However, the desired non-uniformity in magnetization can be created through proper design of sample structure by using single or multiple magnetic materials, and can be controlled through dynamic demagnetizing field with the help of an external magnetic field⁸¹. Very recently, the theoretical work by Krivoruchko et al. have shown that an external electric field, applied along a direction perpendicular to SW wavevector and magnetization, can induce Dzyaloshinskii-Moriya-like (DM-like) interaction⁸², known as Aharanov–Casher effect. This electric field-induced DM-like interaction makes SW-dispersion anisotropic and nonreciprocal, which also promises to be a potential method to create caustic-like SW beam excited from a point source in a FM thin film. Another interesting method is the confinement and channeling SWs along magnetic domain walls of nanometer width. Domain walls can be created either by shape anisotropy of thin film²¹ (Fig. 6c) or by heat-assisted magnetic scanning probe lithography technique²². The SW path can be moved along the width of WG by shifting the domain wall by changing bias magnetic field magnitude. Very recently, it has been proposed that by controlling the phase of an array of antenna, the excited SWs can be sent toward any direction and even can be focused at a specific point⁸³. Here, the directional propagation of SWs is achieved by utilizing SW interference phenomena. Alternatively, directional propagation of SWs may also be achieved by tuning propagating SW phase by VCMA (Fig. 6d).

By performing micromagnetic simulations Rana et al. have proposed that propagating SWs can also be confined and guided through virtual nanochannels formed by VCMA¹⁷. This can be done by placing a metallic gate electrode, with width smaller than that of the WG, on top of the WG. When DC voltage is applied across the gate electrode and WG, the electric field at the FM/oxide interface modulates iPMA of WG underneath the gate electrode (Fig. 6e). This creates a virtual channel on the WG with different anisotropy energy than that of the WG. The SWs can propagate along these channels provided that SW resonance condition is satisfied only inside the channels, whereas outside of channels SWs are prohibited at the excitation frequency. The width and shape of the channel is decided by the width and shape of gate electrode. SW nanochannels with width down to few tens of nanometer can be formed by this method (Fig. 6f). The key advantage is that the nanochannels formed by VCMA are

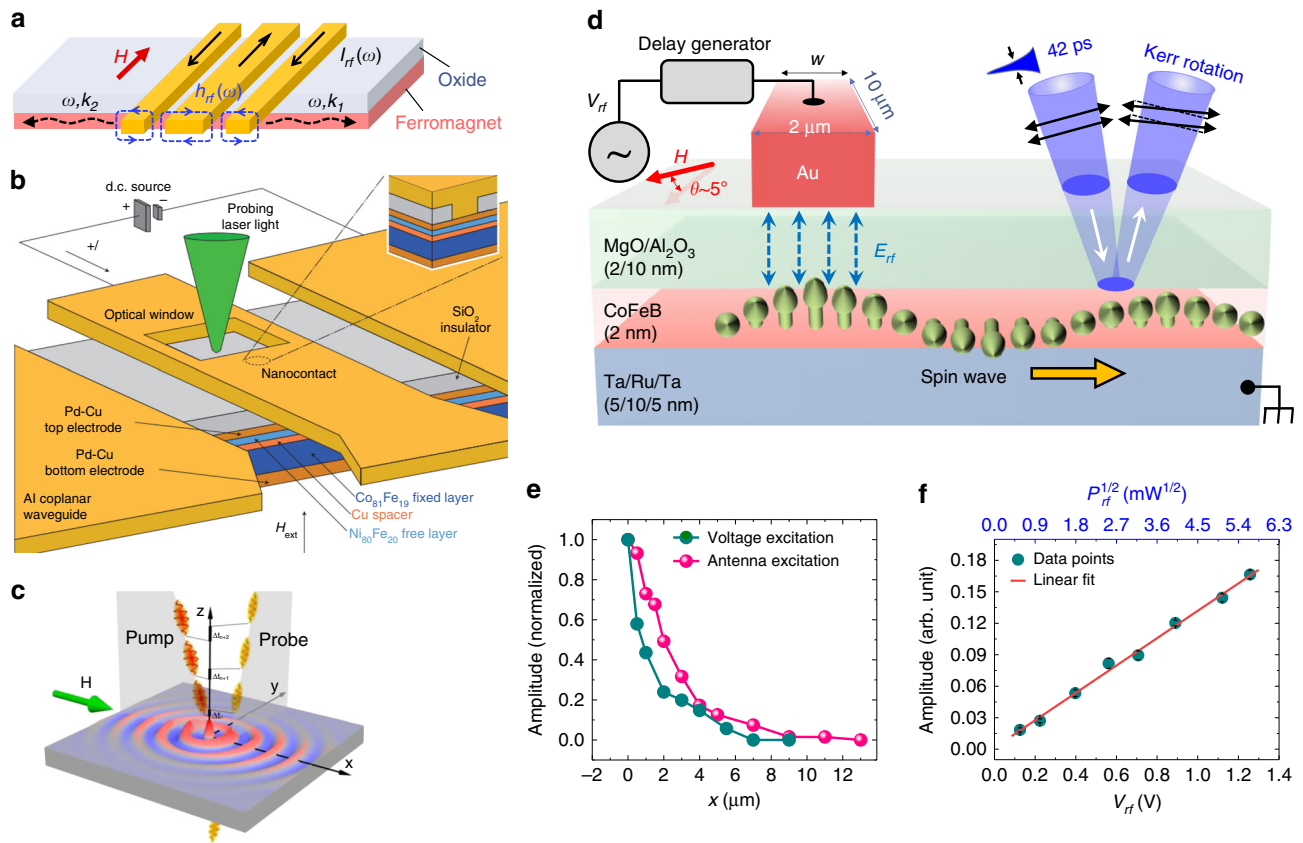


Fig. 5 Excitation of coherent propagating spin waves (SWs). Schematic diagrams show SW excitation by various means. **a** When radio frequency (rf) current is sent through a microwave antenna, the generated Oersted field inductively couples to the SWs having same frequency (ω) as the rf current. The wavelengths of the SWs are decided by the periodicity of nonuniform Oersted field. **b** When an unpolarized current is sent through a ferromagnetic layer (fixed layer), the current is spin-polarized due to the exchange interaction of moving electron spins with the localized magnetic spins in ferromagnet. If this spin-polarized current enters into a second ferromagnetic layer (free layer) through a nanocontact, it locally introduces a torque (known as spin-transfer torque) into the magnetic moments and excites SWs, which can propagate along the ferromagnetic layer¹³. Reprinted by permission from Springer Nature: Nature Nanotechnology, Direct observation of a propagating spin wave induced by spin-transfer torque., Madami, M., Bonetti, S., Consolo, G., Tacchi, S., Carloti, G., Gubbiotti, G., Mancoff, F. B., Yar, M. A., Akerman, J., copyright 2011. **c** Femtosecond laser pulses can partially or fully demagnetize an ordered magnetic material within sub-picosecond time scale and efficiently excite coherent propagating SWs¹⁵ (licensed under CC BY 4.0). **d** If the interfacial perpendicular magnetic anisotropy (iPMA) of an ultrathin ferromagnetic film is locally modulated by applying a microwave voltage across a metal gate electrode and waveguide, propagating SWs are excited when frequency of microwave voltage equals to the SW frequency¹. **e** Decay of SW amplitude with propagation distance excited by voltage-controlled magnetic anisotropy (VCMA) and microwave antenna. Reprinted from Rana, B., Fukuma, Y., Miura, K., Takahashi, H. & Otani, Y. Excitation of coherent propagating SWs in ultrathin CoFeB film by voltage-controlled magnetic anisotropy, *Appl. Phys. Lett.* **111**, 052404 (2017), with the permission of AIP Publishing. **f** Linear variation of VCMA-induced SW amplitude with radio frequency voltage (V_{rf})¹. Reprinted from Rana, B., Fukuma, Y., Miura, K., Takahashi, H. & Otani, Y. Excitation of coherent propagating SWs in ultrathin CoFeB film by voltage-controlled magnetic anisotropy, *Appl. Phys. Lett.* **111**, 052404 (2017), with the permission of AIP Publishing

reconfigurable. It means a number of channels can be formed simultaneously for parallel data processing, and SWs can be selectively sent through any single channel or any combination of channels. Moreover, the SWs with different wavevector can be sent through different channels when the channels are formed by applying different gate voltages. Sadovnikov et al. have demonstrated that the SWs propagating along a stripe-like WG can be transferred to an identical adjacent magnetic stripe through dynamic dipolar coupling between the stripes⁸⁴. By controlling the internal magnetic field of stripes through voltage-induced strain, one can tune the dipolar interaction between the SWs propagating along bilateral magnonic stripes. In that way, the channeling of SWs through magnonic stripe and transfer of SW signals from one magnonic stripe to other one can be reconfigured by gate voltage.

One of the main sources of power consumption in magnonic devices is bias magnetic field, which is generally created by

sending current through the coil. This problem can be solved if ultrathin FM films with relatively high iPMA are used. The iPMA helps to align magnetization perpendicular to the plane of the film even in absence of bias magnetic field. Therefore, the nanochannels can be formed even in absence of bias magnetic field. It is worth to mention here that magnetostatic forward volume spin waves (MSFVWs) are excited when the magnetization of thin film is aligned perpendicular to the plane, and this MSFVWs can easily propagate through a curved path due to their isotropic dispersion character as opposed to other magnetostatic waves excited for in-plane orientation of magnetization⁸⁵. Halder et al. have demonstrated another alternative method for SW transmission without bias magnetic field²⁶. If magnetostatically coupled arrays of nanomagnets, which have well-defined orientation of magnetization at remanence due to shape anisotropy, are used as WGs, the SWs can propagate along straight as well as curved path even in absence of bias magnetic field.

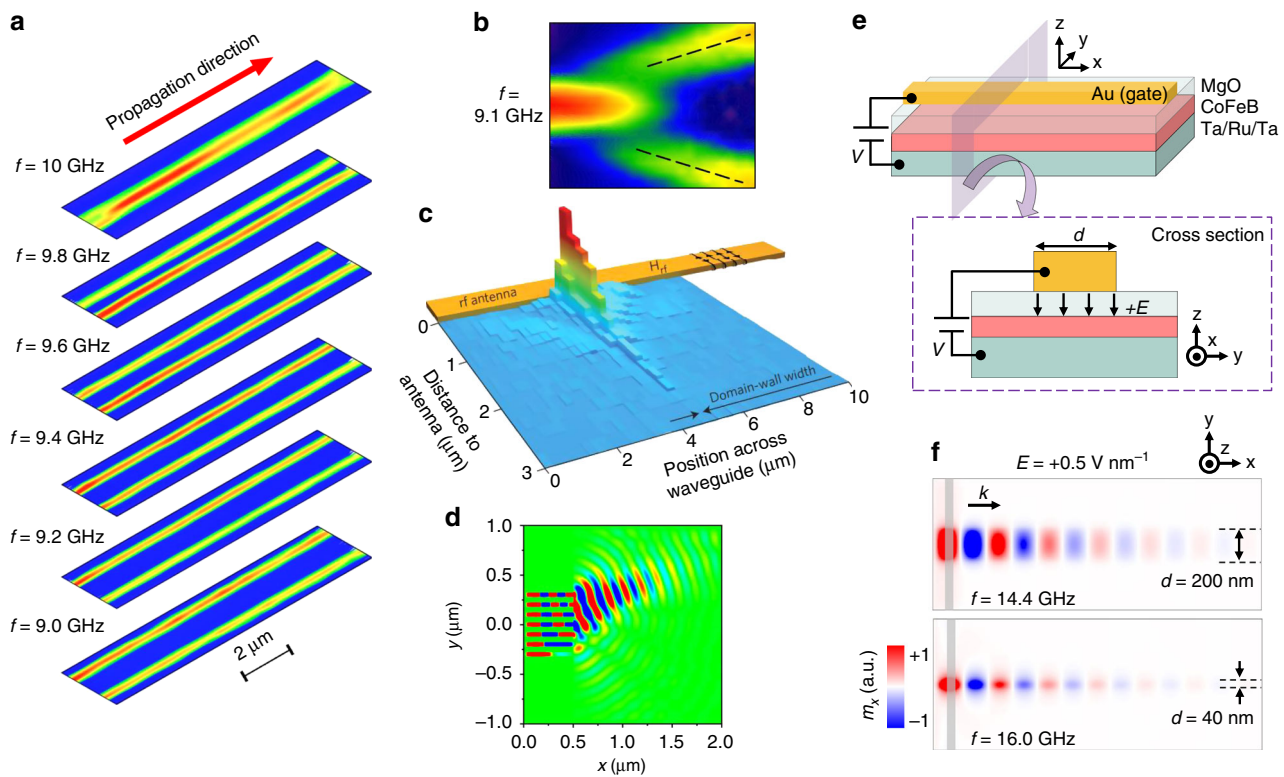


Fig. 6 Reconfigurable spin wave (SW) nanochannels. **a** SW channels formed by internal demagnetizing field⁷⁹. SW channels can be shifted along the width of waveguide (WG) by tuning microwave frequency. Reprinted from Demidov, V. E., Demokritov, S. O., Rott, K., Krzysteczko, P. & Reiss, G. Nano-optics with SWs at microwave frequencies. *Appl. Phys. Lett.* **92**, 232503 (2008), with the permission of AIP Publishing. **b** Radiation of SWs from narrower WG to much wider WG along well-defined direction²⁰. Reproduced with the permission from <https://doi.org/10.1103/PhysRevB.80.014429>. **c** Propagation of SWs along sub-micrometer size magnetic domain wall²¹. Reprinted by permission from Springer Nature: *Nature Nanotechnology*, Magnetic domain walls as reconfigurable spin-wave nanochannels, Wagner, K., Kákay, A., Schultheiss, K., Henschke, A., Sebastian, T., Schultheiss, H., copyright 2016. **d** Directional propagation of SWs by controlling SW phase through voltage-controlled magnetic anisotropy (VCMA)⁸³. Reproduced with the permission from <https://doi.org/10.1103/PhysRevApplied.11.024027>. **e** Principle of nanochannel formation on an ultrathin ferromagnetic (FM) film by VCMA. Adapted with the permission from <https://doi.org/10.1103/PhysRevApplied.9.014033>. **f** Simulated spatial maps of dynamic magnetization show the confinement of propagating SWs in virtual nanochannels formed by VCMA¹⁷. Adapted with the permission from <https://doi.org/10.1103/PhysRevApplied.9.014033>

Reconfigurable magnonic crystals

Manipulation of SW properties such as SW frequency, wavevector, phase, group velocity, amplitude, attenuation length, and magnonic band structure are essential for the development of magnonic logic devices, filters, attenuators, and amplifiers. Charge current-induced Oersted field has been one of the most commonly used techniques for modulation of SW frequency, wavevector, and phase. Nagaoka et al.¹⁸ have shown that the frequency of propagating SWs in FM films possessing iPMA can be modulated by VCMA without charge current. Although there are some reports about the electric-field modulation of SWs in multiferroic materials^{27,28} and ferrimagnetic insulators (e.g. YIG)^{82,86}, the VCMA modulation of SWs in metallic FMs has several advantages over them as already discussed.

Magnonic crystals (MCs) are the artificial crystals, which are formed by periodic spatial variation of magnetic parameters of a magnetic thin film. MCs are used to manipulate the magnonic band structure and/or to create and tune magnonic band gaps of a magnonic WG with respect to the magnonic band structure of a plain WG⁸⁷ (Fig. 7a). This is essential in order to develop various magnonic filters, attenuators, and logic devices. There are several ways to create MCs as described in an interesting review article by Chumak et al.⁸⁸. Static MCs can be created by periodic variation of film thickness, width, and shape of WG⁸⁹, saturation magnetization, and anisotropy⁹⁰. Arrays of magnetic dots^{72,91} and antidots^{87,92} are examples of static MCs. The magnonic zone

boundaries and band gaps of static MCs can be tuned only by external bias magnetic field⁸⁹, which is not very easy to utilize in practical devices. Dynamic MCs can be created by periodic arrays of stripe domain structures at the remanence state⁹³, laser-induced periodic heating⁹⁴ (which modifies saturation magnetization), current-induced periodic Oersted field⁹⁵ (Fig. 7b), and travelling surface acoustic wave-induced periodic strain⁹⁶ (Doppler shift of SW frequency). The magnonic bands of dynamic MCs can be reconfigured easily as compared with static MCs. Moreover, same dynamic MC can be used for multi-purposes, such as logic operations, magnonic conduits, reconfigurable filters, and data reversers. Wang et al. recently proposed reconfigurable MCs created by VCMA⁹⁷. MCs can be created artificially by placing periodic arrays of stripe-like metal gate electrodes on top of an ultrathin FM film (Fig. 7c). When DC voltage is applied across gate electrodes and WG, the iPMA of FM, only underneath the gate electrodes, is modulated by static electric field applied at FM/oxide interface. As a result, MC is developed with a lattice constant same as the spatial periodicity of gate electrodes. The Brillouin zone boundary of this MC, which is decided by the periodicity (P) of modulated iPMA, can be shifted by changing the periodicity of applied gate voltage. This voltage-controlled MC can open a magnonic band gap at Brillouin zone boundary, where propagation of SWs is prohibited due to reflection from zone boundary (Fig. 7d). The key advantage of VCMA-controlled MCs is that the width of the band gap and transmission of SWs at

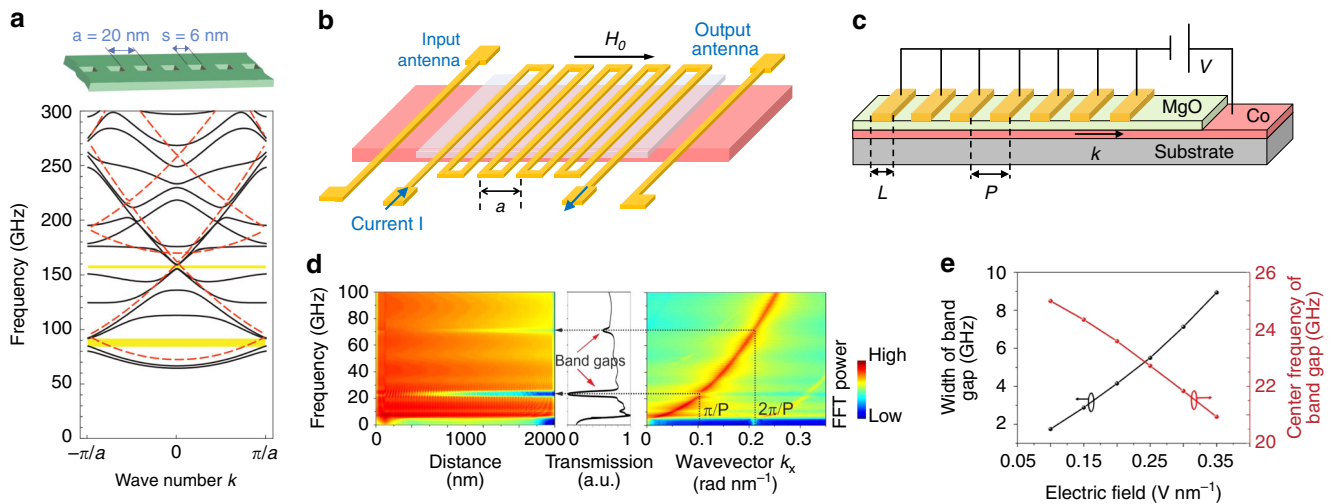


Fig. 7 Magnonic crystals. **a** Calculated magnonic dispersion curves for 1D array of square magnetic antidots as shown in top panel (solid lines) and waveguide (WG) without antidots (dashed lines). Yellow horizontal lines represent magnonic band gaps of antidot lattice⁸⁷. Adapted with the permission from <https://doi.org/10.1103/PhysRevB.89.014406>. **b** Dynamic magnonic crystal (MC) created by spatially varying magnetic field⁹⁵. **c** Schematic diagram of a voltage-controlled MC. Electric field is applied across periodically arranged stripe-like metal gates and WG to tune interfacial perpendicular magnetic anisotropy (iPMA) of WG⁹⁷. **d** Frequency spectra of transmitted spin waves (SWs) and the corresponding dispersion curve for applied electric field $E = 2 \text{ V nm}^{-1}$. Band gaps are observed at zone boundaries $k_x = \pi/P, 2\pi/P$, where transmission of SWs is significantly reduced. Here, k_x is the SW wavevector along x-axis, and P is the spatial periodicity of applied electric field. Reproduced with the permission from <https://doi.org/10.1103/PhysRevB.95.134433>. **e** Variation of magnonic band width and band frequency with gate voltage. Reproduced with the permission from <https://doi.org/10.1103/PhysRevB.95.134433>

Brillouin zone boundary can be tuned by varying gate voltage magnitude (Fig. 7e). This shows the reconfigurable character of these MCs. Moreover, the MC and corresponding band gap at zone boundary can be turned on and off in nanosecond time scale at a very low power consumption.

VCMA-controlled magnonic interferometers for logic operations

In electronics, the digital operations are performed by using various kinds of logic gates made of transistors. Likewise, the digital operations in magnonics can be performed by using magnonic logic gates made of magnonic interferometers and magnonic transistors. Magnonic interferometers are based on the wave characters of SWs, whereas magnonic transistors are based on the particles characters of magnons. Mach-Zehnder interferometer (MZI) is widely used for SW interference operations. Two SWWGs are used as two arms of MZI. The SWs in these two arms are launched either from a single source or from two independent sources, and then the SWs are interfered either physically⁹⁸ or electronically¹⁹. The SW amplitude and/or phase in these two arms are manipulated by external perturbations to control the output interference signal⁷. Anything which can modulate SW properties can be used as external perturbations, such as current-induced Oersted field^{16,19,98}, heat⁹⁴, and VCMA¹⁷. In logic operation, the external perturbations are used as logic inputs, and interference signal is used as logic output. For example, logic inputs may be defined to be “1” when perturbations are “on” (i.e. current through conductor or voltage across the gates are applied) and “0” when perturbations are “off”. Likewise, logic output may be defined to be “1” when large SW signal is obtained due to constructive interference, and “0” when minimal SW signal is obtained due to destructive interference. In another approach, SW phase itself is used as logic inputs⁹⁹. For instance, SW phase “0” and “ π ” can be used as logic inputs “0” and “1”, respectively. All kinds of logic gates such as NOT, AND, OR, NOR, XNOR, NAND, and majority gate can be realized by using single or multiple SW interferometers. The main drawbacks

of Oersted field-controlled MZIs are higher power consumption and difficulty to implement in nanoscale magnonic devices due to nonlocalized nature of Oersted field. These two problems can be resolved if the interferometer is operated by VCMA. Rana et al. have proposed VCMA-controlled XNOR, universal NAND logic gates¹⁷. Interfacial PMA of the two WGs, used as the arms of MZI, are locally modulated by applying voltage across metal gate and WG (Fig. 8a). The applied gate voltage either modulates SW phase or stop SW propagation depending upon its sign and magnitude. The XNOR gate can be developed by modulating SW phase (Fig. 8b), whereas universal NAND gate can be developed by stopping SW propagation. In addition, universal NAND gate can also be formed by using VCMA-controlled SW nanochannels. Chumak et al. reported all-magnon-based logic devices, where it has been shown that the source-to-drain magnon current (i.e., SWs) in a magnon transistor can be controlled by launching additional magnons from an intermediate gate¹⁰⁰. The high density of magnons confined in gate area ensures nonlinear four magnon scattering. Therefore, the magnon current at the output of drain is dramatically reduced with the injection of gate magnons. The advantage of this magnon transistor is that the SWs are not controlled by charge current induced methods. If the source and gate magnons are generated by VCMA^{1,70}, the power consumption may be drastically reduced. The XOR (Fig. 8c) and universal NAND gates can be formed by combining two such magnon transistors in parallel. Another component of magnonic logic devices is SW multiplexer and demultiplexer, which are basically used to send SW signal from one of the many input channels to one of the many output channels via a combiner. These devices can also be formed by either Oersted field⁷⁸ or VCMA¹⁷.

Future perspectives

Magnetolectric effect, especially, VCMA is a very powerful method to excite, manipulate, channel SWs, and to develop nanoscale magnonic logic devices by electric field with ultralow power consumption. Although many theoretical and simulation

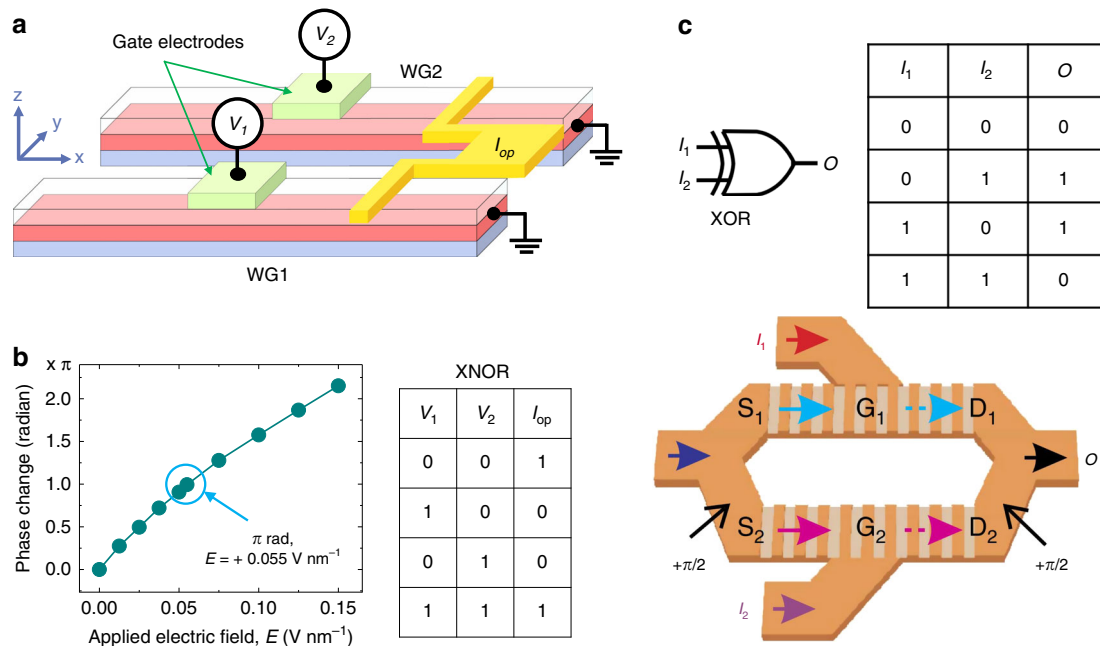


Fig. 8 Magnonic logic gates. **a** Schematic illustration of a voltage-controlled magnetic anisotropy (VCMA)-controlled exclusive NOR (XNOR) logic gate based upon Mach-Zehnder interferometer (MZI). **b** The graph shows the variation of spin wave (SW) phase in one waveguide (WG) with gate voltage¹⁷. Adapted with the permission from <https://doi.org/10.1103/PhysRevApplied.9.014033>. **c** Schematic diagram of an exclusive OR (XOR) logic gate made by combining two magnon transistors in parallel¹⁰⁰. The output signal “O” is manipulated by tuning magnon currents in two arms of the logic gate by feeding magnon current from two independent gates (G_1 , G_2). Reprinted by permission from Springer Nature: *Nature Communications*, Magnon transistor for all-magnon data processing, Chumak, A. V., Serga, A. A. & Hillebrands, B., copyright 2014

results are reported on the various functions of magnonic devices by VCMA, the experimental demonstration and study for most of them are still lacking. As the theoretical and simulations results do not take into account electrical losses due to leakage current and impedance mismatch, experimental studies are essential to figure out and minimize the electrical losses by proper engineering of magnonic devices. For instance, Nozaki et al. have reported that majority of microwave power is reflected from a MTJ due to impedance mismatch⁶³. A major bottleneck in practical realization of electric-field-controlled magnonic devices is low value of VCMA coefficient. Therefore, increasing VCMA coefficient up to $pJ\ V^{-1}m^{-1}$ by engineering FM/oxide interface is of high priority. Another bottleneck is to find out FM materials with low damping parameter in order to reduce energy loss of SWs. Ferrimagnetic insulators and Heusler alloys can be the alternatives. Experimental report shows that a direct electric field coupling to propagating SWs is possible even in a centrosymmetric ferrimagnetic insulators, like YIG, via Aharonov–Casher effect. This provides an efficient way to modulate SW frequency, phase⁸⁶, and propagation direction⁸². Although, Heusler alloys, like Co_2FeAl , show iPMA¹⁰¹ and high TMR¹⁰², demonstration of electric-field control of iPMA is still lacking. As a matter of fact, FMs are suitable for applying VCMA. Therefore, use of SW amplifier is essential in magnonic devices to compensate the energy losses of SWs during propagation. There are several well-known charge current induced methods available for SW amplification. For instance, the SWs can be amplified by passing current through conducting WG⁷⁷, by microwave magnetic field through parametric pumping²⁴, by modulating Gilbert damping through spin-orbit torque (SOT)^{2,3,23}, which can be even modulated by electric field¹⁰³. Alternatively, VCMA can be used for SWs amplification in order to design low power magnonic devices. Microwave magnetic field can be replaced by VCMA-torque to build up energy-efficient parametric amplifier. Although magnetoelectric coupling in synthetic multiferroic

structure can be used for electric-field-controlled parametric amplifier²⁵, VCMA has some additional advantages over them in terms of localization area which can be as small as few tens of nanometer. The VCMA can also amplify the SWs in metallic FM by reducing Gilbert damping parameter⁴⁴. As the use of ultrathin FM films is essential for reducing dimension of magnonic devices and controlling interfacial magnetic properties, it is important to study the SW properties in ultrathin FM films. Electrical detection of SWs is required for practical applications. SW detection by microwave antenna through inductive coupling becomes very inefficient method, especially, for ultrathin films possessing iPMA. MTJs which have proven to be a very sensitive method for reading data in modern magnetic recording media and detecting FMR, could be an alternative way to detect SWs in ultrathin films. Recently, magnetic Skyrmions which are non-trivial nanoscale topological chiral spin structures, promise to have huge potential for the application as a high-density data storage and as an information carrier. Skyrmion size, nucleation field, and dynamic modes can be controlled by VCMA¹⁰⁴. Moreover, SWs can drive Skyrmions by SOT at ultralow power consumption¹⁰⁵ through a virtual channel created by VCMA¹⁰⁶. These results show the possibility of combining Skyrmions into VCMA-controlled magnonics devices.

Data availability

The related data are available from the corresponding authors on request.

Received: 31 October 2018 Accepted: 28 June 2019

Published online: 01 August 2019

References

1. Rana, B., Fukuma, Y., Miura, K., Takahashi, H. & Otani, Y. Excitation of coherent propagating spin waves in ultrathin CoFeB film by voltage-controlled magnetic anisotropy. *Appl. Phys. Lett.* **111**, 052404 (2017). **First experimental**

- report on spin wave excitation by voltage-controlled magnetic anisotropy and its advantages over Oersted field excitation.**
2. Divinskiy, B. et al. Excitation and amplification of spin waves by spin-orbit torque. *Adv. Mater.* **30**, 1802837 (2018).
 3. Evelt, M. et al. High-efficiency control of spin-wave propagation in ultra-thin yttrium iron garnet by the spin-orbit torque. *Appl. Phys. Lett.* **108**, 172406 (2016).
 4. Kajiwara, Y. et al. Transmission of electrical signals by spin-wave interconversion in a magnetic insulator. *Nature* **464**, 262–266 (2010).
 5. Stamps, R. L. & Camley, R. E. Spin waves in antiferromagnetic thin films and multilayers: Surface and interface exchange and entire-cell effective-medium theory. *Phys. Rev. B* **54**, 15200–15209 (1996).
 6. Kruglyak, V. V., Demokritov, S. O. & Grundler, D. Magnonics. *J. Phys. D: Appl. Phys.* **43**, 260301 (2010).
 7. Khitun, A., Bao, M. & Wang, K. L. Magnonic logic circuits. *J. Phys. D: Appl. Phys.* **43**, 264005 (2010).
 8. Lenk, B., Ulrichs, H., Garbs, F. & Münzenberg, M. The building blocks of magnonics. *Phys. Rep.* **507**, 107–136 (2011).
 9. Chumak, A. V., Vasyuchka, V. I., Serga, A. A. & Hillebrands, B. Magnon spintronics. *Nat. Phys.* **11**, 453–461 (2015). **A review article on the development of spintronics devices by utilizing magnons i.e. quanta of spin waves.**
 10. Barman, A. & Sinha, J. *Spin Dynamics and Damping in Ferromagnetic Thin Films and Nanostructures* (Springer, Cham, Switzerland, 2017).
 11. Rana, B. & Barman, A. Magneto-optical measurements of collective spin dynamics of two-dimensional arrays of ferromagnetic nanoelements. *SPIN* **03**, 1330001 (2013).
 12. Demidov, V. E. et al. Excitation of coherent propagating spin waves by pure spin currents. *Nat. Commun.* **7**, 10446 (2016).
 13. Madami, M. et al. Direct observation of a propagating spin wave induced by spin-transfer torque. *Nat. Nanotechnol.* **6**, 635–638 (2011).
 14. Vlaminck, V. & Bailleul, M. Spin-wave transduction at the submicrometer scale: experiment and modeling. *Phys. Rev. B* **81**, 014425 (2010).
 15. Savochkin, I. V. et al. Generation of spin waves by a train of fs-laser pulses: a novel approach for tuning magnon wavelength. *Sci. Rep.* **7**, 5668 (2017).
 16. Schneider, T. et al. Realization of spin-wave logic gates. *Appl. Phys. Lett.* **92**, 022505 (2008).
 17. Rana, B. & Otani, Y. Voltage-controlled reconfigurable spin-wave nanochannels and logic devices. *Phys. Rev. Appl.* **9**, 014033 (2018). **Proposal of voltage-controlled reconfigurable nanochannels for spin wave propagation and its application towards the development of logic gates.**
 18. Nawaoka, K. et al. Voltage modulation of propagating spin waves in Fe. *J. Appl. Phys.* **117**, 17A905 (2015).
 19. Rousseau, O. et al. Realization of a micrometre-scale spin-wave interferometer. *Sci. Rep.* **5**, 9873 (2015).
 20. Demidov, V. E. et al. Radiation of spin waves from the open end of a microscopic magnetic-film waveguide. *Phys. Rev. B* **80**, 014429 (2009).
 21. Wagner, K. et al. Magnetic domain walls as reconfigurable spin-wave nanochannels. *Nat. Nanotechnol.* **11**, 432–436 (2016).
 22. Albisetti, E. et al. Nanoscale spin-wave circuits based on engineered reconfigurable spin-textures. *Commun. Phys.* **1**, 56 (2018).
 23. Gladii, O. et al. Spin wave amplification using the spin Hall effect in permalloy/platinum bilayers. *Appl. Phys. Lett.* **108**, 202407 (2016).
 24. Bao, M. et al. Coplanar waveguide radio frequency ferromagnetic parametric amplifier. *Appl. Phys. Lett.* **93**, 072509 (2008).
 25. Khitun, A., Nikonov, D. E. & Wang, K. L. Magnetolectric spin wave amplifier for spin wave logic circuits. *J. Appl. Phys.* **106**, 123909 (2009).
 26. Haldar, A., Kumar, D. & Adeyeye, A. O. A reconfigurable waveguide for energy-efficient transmission and local manipulation of information in a nanomagnetic device. *Nat. Nanotechnol.* **11**, 437–443 (2016).
 27. Zhu, M. et al. Modulation of spin dynamics via voltage control of spin-lattice coupling in multiferroics. *Adv. Funct. Mater.* **27**, 1605598 (2017).
 28. Rovillain, P. et al. Electric-field control of spin waves at room temperature in multiferroic BiFeO₃. *Nat. Mater.* **9**, 975–979 (2010).
 29. Tong, W.-Y., Fang, Y.-W., Cai, J., Gong, S.-J. & Duan, C.-G. Theoretical studies of all-electric spintronics utilizing multiferroic and magnetoelectric materials. *Comput. Mater. Sci.* **112**, 467–477 (2016).
 30. Ohno, H. et al. Electric-field control of ferromagnetism. *Nature* **408**, 944–946 (2000).
 31. Xu, M. et al. Inverse Edelstein effect induced by magnon-phonon coupling. *Phys. Rev. B* **97**, 180301(R) (2018).
 32. Diény, B. & Chshiev, M. Perpendicular magnetic anisotropy at transition metal/oxide interfaces and applications. *Rev. Mod. Phys.* **89**, 025008 (2017). **A complete review on the perpendicular magnetic anisotropy at the interfaces of transition metals and various oxides: its origin, properties, controlling parameters, importance and potential applications.**
 33. Duan, C. et al. Surface magnetoelectric effect in ferromagnetic metal films. *Phys. Rev. Lett.* **101**, 137201 (2008).
 34. Tsujikawa, M. & Oda, T. Finite electric field effects in the large perpendicular magnetic anisotropy surface Pt/Fe/Pt(001): a first-principles study. *Phys. Rev. Lett.* **102**, 247203 (2009). **First principle calculation results to understand the effect of applied electric field on interfacial magnetic anisotropy.**
 35. Pal, S., Rana, B., Hellwig, O., Thomson, T. & Barman, A. Tunable magnonic frequency and damping in [Co/Pd]_s multilayers with variable Co layer thickness. *Appl. Phys. Lett.* **98**, 082501 (2011).
 36. Ikeda, S. et al. A perpendicular-anisotropy CoFeB–MgO magnetic tunnel junction. *Nat. Mater.* **9**, 721–724 (2010).
 37. Ikeda, S. et al. Tunnel magnetoresistance of 604% at 300K by suppression of Ta diffusion in CoFeB/MgO/CoFeB pseudo-spin-valves annealed at high temperature. *Appl. Phys. Lett.* **93**, 082508 (2008).
 38. Kawabe, T. et al. Electric-field-induced changes of magnetic moments and magnetocrystalline anisotropy in ultrathin cobalt films. *Phys. Rev. B* **96**, 220412 (2017).
 39. Miwa, S. et al. Voltage controlled interfacial magnetism through platinum orbits. *Nat. Commun.* **8**, 15848 (2017).
 40. Barnes, S. E., Ieda, J. & Maekawa, S. Rashba spin-orbit anisotropy and the electric field control of magnetism. *Sci. Rep.* **4**, 4105 (2014).
 41. Naik, V. B. et al. Effect of electric-field on the perpendicular magnetic anisotropy and strain properties in CoFeB/MgO magnetic tunnel junctions. *Appl. Phys. Lett.* **105**, 052403 (2014).
 42. Xiang, Q. et al. Nonlinear electric field effect on perpendicular magnetic anisotropy in Fe/MgO interfaces. *J. Phys. D: Appl. Phys.* **50**, 40LT04 (2017).
 43. Kanai, S., Gajek, M., Worledge, D. C., Matsukura, F. & Ohno, H. Electric field-induced ferromagnetic resonance in a CoFeB/MgO magnetic tunnel junction under dc bias voltages. *Appl. Phys. Lett.* **105**, 242409 (2014).
 44. Okada, A. et al. Electric-field effects on magnetic anisotropy and damping constant in Ta/CoFeB/MgO investigated by ferromagnetic resonance. *Appl. Phys. Lett.* **105**, 052415 (2014).
 45. Shiota, Y. et al. Opposite signs of voltage-induced perpendicular magnetic anisotropy change in CoFeB/MgO junctions with different underlayers. *Appl. Phys. Lett.* **103**, 082410 (2013).
 46. Miura, K. et al. Voltage-induced magnetization dynamics in CoFeB/MgO/CoFeB magnetic tunnel junctions. *Sci. Rep.* **7**, 42511 (2017).
 47. Rana, B., Fukuma, Y., Miura, K., Takahashi, H. & Otani, Y. Effect of excitation power on voltage induced local magnetization dynamics in an ultrathin CoFeB film. *Sci. Rep.* **7**, 2318 (2017).
 48. Nozaki, T. et al. Voltage-induced magnetic anisotropy changes in an ultrathin FeB layer sandwiched between two MgO layers. *Appl. Phys. Express* **6**, 073005 (2013).
 49. Kozioł-Rachwał, A. et al. Enhancement of perpendicular magnetic anisotropy and its electric field-induced change through interface engineering in Cr/Fe/MgO. *Sci. Rep.* **7**, 5993 (2017).
 50. Skowronski, W. et al. Underlayer material influence on electric-field controlled perpendicular magnetic anisotropy in CoFeB/MgO magnetic tunnel junctions. *Phys. Rev. B* **91**, 184410 (2015).
 51. Yohei, H. et al. Electric-field effect on magnetic anisotropy in Pt/Co/Pd/MgO structures deposited on GaAs and Si substrates. *Appl. Phys. Express* **11**, 013003 (2018).
 52. Hibino, Y. et al. Peculiar temperature dependence of electric-field effect on magnetic anisotropy in Co/Pd/MgO system. *Appl. Phys. Lett.* **109**, 082403 (2016).
 53. Lam, D. D. et al. MgO overlayer thickness dependence of perpendicular magnetic anisotropy in CoFeB thin films. *J. Korean Phys. Soc.* **62**, 1461–1464 (2013).
 54. Tsujikawa, M., Haraguchi, S. & Oda, T. Effect of atomic monolayer insertions on electric-field-induced rotation of magnetic easy axis. *J. Appl. Phys.* **111**, 083910 (2012).
 55. Li, X. et al. Enhancement of voltage-controlled magnetic anisotropy through precise control of Mg insertion thickness at CoFeB/MgO interface. *Appl. Phys. Lett.* **110**, 052401 (2017).
 56. Nozaki, T. et al. Enhancement in the interfacial perpendicular magnetic anisotropy and the voltage-controlled magnetic anisotropy by heavy metal doping at the Fe/MgO interface. *APL Mater.* **6**, 026101 (2018).
 57. Witold, S. et al. Perpendicular magnetic anisotropy of Ir/CoFeB/MgO trilayer system tuned by electric fields. *Appl. Phys. Express* **8**, 053003 (2015).
 58. Rajanikanth, A., Hauet, T., Montaigne, F., Mangin, S. & Andrieu, S. Magnetic anisotropy modified by electric field in V/Fe/MgO(001)/Fe epitaxial magnetic tunnel junction. *Appl. Phys. Lett.* **103**, 062402 (2013).
 59. Bauer, U. et al. Magneto-ionic control of interfacial magnetism. *Nat. Mater.* **14**, 174 (2014).
 60. Bauer, U., Przybylski, M., Kirschner, J. & Beach, G. S. D. Magnetoelectric charge trap memory. *Nano Lett.* **12**, 1437–1442 (2012).
 61. Yu, G. et al. Strain-induced modulation of perpendicular magnetic anisotropy in Ta/CoFeB/MgO structures investigated by ferromagnetic resonance. *Appl. Phys. Lett.* **106**, 072402 (2015).

62. Zhu, J. et al. Voltage-induced ferromagnetic resonance in magnetic tunnel junctions. *Phys. Rev. Lett.* **108**, 197203 (2012).
63. Nozaki, T. et al. Electric-field-induced ferromagnetic resonance excitation in an ultrathin ferromagnetic metal layer. *Nat. Phys.* **8**, 491–496 (2012). **Experimental study on the properties of voltage-controlled magnetic anisotropy induced uniform ferromagnetic resonance in ultrathin ferromagnetic films.**
64. Shiota, Y. et al. Field angle dependence of voltage-induced ferromagnetic resonance under DC bias voltage. *J. Magn. Magn. Mater.* **400**, 159–162 (2016).
65. Hirayama, E. et al. Electric-field induced nonlinear ferromagnetic resonance in a CoFeB/MgO magnetic tunnel junction. *Appl. Phys. Lett.* **107**, 132404 (2015).
66. Dobin, A. Y. & Victora, R. H. Intrinsic nonlinear ferromagnetic relaxation in thin metallic films. *Phys. Rev. Lett.* **90**, 167203 (2003).
67. Verba, R., Tiberkevich, V., Krivorotov, I. & Slavin, A. Parametric excitation of spin waves by voltage-controlled magnetic anisotropy. *Phys. Rev. Appl.* **1**, 044006 (2014). **Various properties and advantages of nonlinear parametric excitation of spin waves in ultrathin ferromagnetic films by voltage-controlled magnetic anisotropy.**
68. Verba, R., Carpentieri, M., Finocchio, G., Tiberkevich, V. & Slavin, A. Excitation of spin waves in an in-plane-magnetized ferromagnetic nanowire using voltage-controlled magnetic anisotropy. *Phys. Rev. Appl.* **7**, 064023 (2017).
69. Verba, R., Carpentieri, M., Finocchio, G., Tiberkevich, V. & Slavin, A. Excitation of propagating spin waves in ferromagnetic nanowires by microwave voltage-controlled magnetic anisotropy. *Sci. Rep.* **6**, 25018 (2016).
70. Chen, Y.-J. et al. Parametric resonance of magnetization excited by electric field. *Nano Lett.* **17**, 572–577 (2017).
71. Poimanov, V. D., Kuchko, A. N. & Kruglyak, V. V. Magnetic interfaces as sources of coherent spin waves. *Phys. Rev. B* **98**, 104418 (2018).
72. Rana, B. et al. Detection of picosecond magnetization dynamics of 50 nm magnetic dots down to the single dot regime. *ACS Nano* **5**, 9559–9565 (2011).
73. Satoh, T. et al. Directional control of spin-wave emission by spatially shaped light. *Nat. Photonics* **6**, 662 (2012).
74. Au, Y. et al. Direct excitation of propagating spin waves by focused ultrashort optical pulses. *Phys. Rev. Lett.* **110**, 097201 (2013).
75. Ando, Y. et al. Thermally excited spin wave modes in synthetic antiferromagnetic stripes. *J. Magn. Magn. Mater.* **310**, 1949–1951 (2007).
76. Au, Y. et al. Resonant microwave-to-spin-wave transducer. *Appl. Phys. Lett.* **100**, 182404 (2012).
77. Seo, S.-M., Lee, K.-J., Yang, H. & Ono, T. Current-induced control of spin-wave attenuation. *Phys. Rev. Lett.* **102**, 147202 (2009).
78. Vogt, K. et al. Realization of a spin-wave multiplexer. *Nat. Commun.* **5**, 3727 (2014).
79. Demidov, V. E., Demokritov, S. O., Rott, K., Krzysteczko, P. & Reiss, G. Nano-optics with spin waves at microwave frequencies. *Appl. Phys. Lett.* **92**, 232503 (2008).
80. Davies, C. S. et al. Towards graded-index magnonics: Steering spin waves in magnonic networks. *Phys. Rev. B* **92**, 020408 (2015).
81. Davies, C. S., Poimanov, V. D. & Kruglyak, V. V. Mapping the magnonic landscape in patterned magnetic structures. *Phys. Rev. B* **96**, 094430 (2017).
82. Krivoruchko, V. N., Savchenko, A. S. & Kruglyak, V. V. Electric-field control of spin-wave power flow and caustics in thin magnetic films. *Phys. Rev. B* **98**, 024427 (2018).
83. Song, M., Moon, K.-W., Hwang, C. & Kim, K.-J. Omnidirectional spin-wave array antenna. *Phys. Rev. Appl.* **11**, 024027 (2019).
84. Sadovnikov, A. V. et al. Magnon straintronics: reconfigurable spin-wave routing in strain-controlled bilateral magnetic stripes. *Phys. Rev. Lett.* **120**, 257203 (2018).
85. Klingler, S. et al. Spin-wave logic devices based on isotropic forward volume magnetostatic waves. *Appl. Phys. Lett.* **106**, 212406 (2015).
86. Zhang, X., Liu, T., Flatté, M. E. & Tang, H. X. Electric-field coupling to spin waves in a centrosymmetric ferrite. *Phys. Rev. Lett.* **113**, 037202 (2014).
87. Klos, J. W., Kumar, D., Krawczyk, M. & Barman, A. Influence of structural changes in a periodic antidot waveguide on the spin-wave spectra. *Phys. Rev. B* **89**, 014406 (2014).
88. Chumak, A. V., Serga, A. A. & Hillebrands, B. Magnonic crystals for data processing. *J. Phys. D: Appl. Phys.* **50**, 244001 (2017).
89. Banerjee, C., Choudhury, S., Sinha, J. & Barman, A. Pseudo-one-dimensional magnonic crystals for high-frequency nanoscale devices. *Phys. Rev. Appl.* **8**, 014036 (2017).
90. Grundler, D. Reconfigurable magnonics heats up. *Nat. Phys.* **11**, 438–441 (2015).
91. Saha, S. et al. Tunable magnonic spectra in two-dimensional magnonic crystals with variable lattice symmetry. *Adv. Funct. Mater.* **23**, 2378–2386 (2013).
92. Mandal, R. et al. Optically induced tunable magnetization dynamics in nanoscale Co antidot lattices. *ACS Nano* **6**, 3397–3403 (2012).
93. Banerjee, C. et al. Magnonic band structure in a Co/Pd stripe domain system investigated by Brillouin light scattering and micromagnetic simulations. *Phys. Rev. B* **96**, 024421 (2017).
94. Vogel, M. et al. Optically reconfigurable magnetic materials. *Nat. Phys.* **11**, 487–491 (2015).
95. Chumak, A. V., Neumann, T., Serga, A. A., Hillebrands, B. & Kostylev, M. P. A current-controlled, dynamic magnonic crystal. *J. Phys. D: Appl. Phys.* **42**, 205005 (2009).
96. Chumak, A. V., Dhagat, P., Jander, A., Serga, A. A. & Hillebrands, B. Reverse Doppler effect of magnons with negative group velocity scattered from a moving Bragg grating. *Phys. Rev. B* **81**, 140404 (2010).
97. Wang, Q. et al. Voltage-controlled nanoscale reconfigurable magnonic crystal. *Phys. Rev. B* **95**, 134433 (2017). **Proposal for the development of nanoscale magnonic crystals by applying voltage-controlled magnetic anisotropy and its reconfigurable properties.**
98. Lee, K.-S. & Kim, S.-K. Conceptual design of spin wave logic gates based on a Mach-Zehnder-type spin wave interferometer for universal logic functions. *J. Appl. Phys.* **104**, 053909 (2008).
99. Khitun, A., Bao, M. & Wang, K. L. Spin wave magnetic nanofabric: a new approach to spin-based logic circuitry. *IEEE Trans. Magn.* **44**, 2141–2152 (2008).
100. Chumak, A. V., Serga, A. A. & Hillebrands, B. Magnon transistor for all-magnon data processing. *Nat. Commun.* **5**, 4700 (2014).
101. Wen, Z., Sukegawa, H., Mitani, S. & Inomata, K. Perpendicular magnetization of Co₂FeAl full-Heusler alloy films induced by MgO interface. *Appl. Phys. Lett.* **98**, 242507 (2011).
102. Wen, Z. et al. Magnetic tunnel junctions with perpendicular anisotropy using a Co₂FeAl Full-Heusler Alloy. *Appl. Phys. Express* **5**, 063003 (2012).
103. Chen, L. et al. Electric-field control of interfacial spin-orbit fields. *Nat. Electron.* **1**, 350–355 (2018).
104. Sampaio, J., Cros, V., Rohart, S., Thiaville, A. & Fert, A. Nucleation, stability and current-induced motion of isolated magnetic skyrmions in nanostructures. *Nat. Nanotechnol.* **8**, 839–844 (2013).
105. Iwasaki, J., Beekman, A. J. & Nagaosa, N. Theory of magnon-skyrmion scattering in chiral magnets. *Phys. Rev. B* **89**, 064412 (2014).
106. Upadhyaya, P., Yu, G., Amiri, P. K. & Wang, K. L. Electric-field guiding of magnetic skyrmions. *Phys. Rev. B* **92**, 134411 (2015).

Acknowledgements

This review is supported by Grant-in-Aid for Scientific Research on Innovative Area, “Nano Spin Conversion Science” (grant number 26103002).

Author contributions

B.R. and Y.O. planned the review. B.R. wrote the paper with the inputs from Y.O. Both authors discussed about the contents of the review and corrected the paper.

Additional information

Competing interests: The authors declare no competing interests.

Reprints and permission information is available online at <http://npg.nature.com/reprintsandpermissions/>

Publisher's note: Springer Nature remains neutral with regard to jurisdictional claims in published maps and institutional affiliations.



Open Access This article is licensed under a Creative Commons

Attribution 4.0 International License, which permits use, sharing, adaptation, distribution and reproduction in any medium or format, as long as you give appropriate credit to the original author(s) and the source, provide a link to the Creative Commons license, and indicate if changes were made. The images or other third party material in this article are included in the article's Creative Commons license, unless indicated otherwise in a credit line to the material. If material is not included in the article's Creative Commons license and your intended use is not permitted by statutory regulation or exceeds the permitted use, you will need to obtain permission directly from the copyright holder. To view a copy of this license, visit <http://creativecommons.org/licenses/by/4.0/>.

© The Author(s) 2019